Axisymmetric Acoustic Scattering by Interpolation

Perrin S. Meyer [1], Yu Chen

Courant Institute of Mathematical Sciences, 251 Mercer St., New York University, New York, NY 10012

Abstract

We describe and implement a numerical method for scattering calculation in the exterior of a sound-hard, axisymmetric domain in $\mathbb{R}^3$. Existing methods rely on singularity extraction and separation in order to design high order quadrature formulae, and experience numerical difficulties such as low order convergence [1,2] or instability [3]. Our method does not require a quadrature, is spectrally convergent, and is nearly trivial to program.

1 Introduction

We describe a simple, high-order numerical method for the simulation of sound wave propagation through axisymmetric, sound-hard waveguides. Our underlying problem in application is an axisymmetric musical horn, and we are

Email addresses: perrin@MSLI.com (Perrin S. Meyer), yuchen@courant.nyu.edu (Yu Chen).

[1] Present Address: MSLI Inc., 2832 San Pablo Ave, Berkeley, CA 94702

interested in its optimal design for the far field pattern.

As is well-known, the axisymmetric problem in $\mathbb{R}^3$ can be easily recast as a sequence of obstacle scattering problems in $\mathbb{R}^2$ by means of the rotational symmetry, which in turn is convertible to boundary integral equations; therefore the computational complexity is not an issue even for the highest frequencies (about 20 kHz) at which the size of the horn is typically and considerably less than 1000 wavelengths. The resulting linear system of the boundary integral equation of this size can be directly solved with LU or QR factorizations and on the current hardware.

However, the reduction by rotational symmetry makes the resulting Green's function extremely complicated in terms of algebraic structures of its logarithm singularity, which makes the existing spectrally convergent quadrature formulae difficult to apply. In fact there is no successful effort, to the best of our knowledge, in addressing the puzzling issue of separating the logarithm singularity in the reduced Green's function.

The solution method we present here avoids the separation of the singularity, and at the same time maintains spectral convergence, all at the expense of a higher condition number of the resulting linear system to be solved. The high condition number does not cause any practical stability problem (see §4.5) but the spectral convergence stops when the error of the solution drops to about 10^{-8}.

A major advantage of the new approach is the simplicity of coding. There is no need for us to explicitly design quadratures for singular integrals. In fact, the discretization of the boundary integral equation is more like that for interpolation than for the quadrature.

2 Boundary Integral Equation Formulation

In this section we specify the scattering problem, provide its boundary integral equation formulation, describe the axisymmetry of the sound hard scatterer D, and illustrate the difficulties involved in the quadrature designs.

2.1 Statement of Problem

Let D be a domain in $\mathbb{R}^3$ with smooth boundary ∂D, and let ν be the unit outward normal vector. Given a continuous function g on ∂D, find a radiating solution (the scattered wave) $v \in C^2(\mathbb{R}^3 \setminus \bar{D}) \cap C(\mathbb{R}^3 \setminus D)$, to the Helmholtz equation

$$\triangle v + k^2 v = 0 \quad \text{in } \mathbb{R}^3 \setminus \bar{D} \tag{1}$$

subject to the boundary condition

$$\frac{\partial v}{\partial \nu} = g \quad \text{on } \partial D \tag{2}$$

2.2 Boundary Integral Equation

As is well known [4], the exterior Neumann problem for the Helmholtz equation (1), a well-posed problem, is equivalent to the second–kind boundary integral equation

$$\varphi - K'\varphi - i\eta T\varphi = -2g \tag{3}$$

with η real and nonzero, and with the operators K', T defined by

$$(K'\varphi)(\mathbf{x}) = 2\int_{\partial D} \frac{\partial \Phi(\mathbf{x},\mathbf{y})}{\partial \nu(\mathbf{x})}\varphi(\mathbf{y})\, ds(\mathbf{y}) \quad \mathbf{x} \in \partial D \tag{4}$$

$$(T\varphi)(\mathbf{x}) = 2\frac{\partial}{\partial \nu(\mathbf{x})}\int_{\partial D} \frac{\partial \Phi(\mathbf{x},\mathbf{y})}{\partial \nu(\mathbf{y})}\varphi(\mathbf{y}) ds(\mathbf{y}), \quad \mathbf{x} \in \partial D \tag{5}$$

where Φ is the free space Green's function

$$\Phi(\mathbf{x}, \mathbf{y}) = \frac{1}{4\pi} \frac{e^{ik|\mathbf{x}-\mathbf{y}|}}{|\mathbf{x}-\mathbf{y}|} \tag{6}$$

The scattered filed v can then be recovered from φ via the formula

$$v(\mathbf{x}) = \int_{\partial D} \left(\Phi(\mathbf{x}, \mathbf{y}) \varphi(\mathbf{y}) + i\eta \frac{\partial \Phi(\mathbf{x}, \mathbf{y})}{\partial \nu(\mathbf{y})} \varphi(\mathbf{y}) \right) ds(\mathbf{y}) \tag{7}$$

2.3 Axisymmetric Reformulation

In the remainder of the paper, we will assume that D and g (see §2.1) are axisymmetric around the x-axis. More specifically, let

$$\Gamma = \{ \, (x(t), y(t)) \mid t \in [0, 2\pi] \, \} \tag{8}$$

be a simple, smooth curve on the xy-plane. Denote by Ω the bounded domain in $\mathbb{R}^2$ bounded by Γ. Let the axisymmetric surface ∂D be formed by the rotation of this curve around the x-axis

$$\partial D = \{ \, \mathbf{y}(t, \theta) \in \mathbb{R}^3 \mid \mathbf{y}(t, \theta) = (x(t), y(t) \cos\theta, y(t) \sin\theta) \, \} \tag{9}$$

which is parameterized by $(t, \theta) \in [0, 2\pi] \times [0, 2\pi]$. Let $\mathbf{x}, \mathbf{y}$ be two arbitrary points on ∂D with

$$\mathbf{x}(t, \theta) = x(t)\hat{x} + y(t)\cos(\theta)\hat{y} + y(t)\sin(\theta)\hat{z} \tag{10}$$

$$\mathbf{y}(\tau, \phi) = x(\tau)\hat{x} + y(\tau)\cos(\phi)\hat{y} + y(\tau)\sin(\phi)\hat{z} \tag{11}$$

Then

$$\begin{aligned} R(t, \tau, \theta, \phi) &= |\mathbf{x}(t, \theta) - \mathbf{y}(\tau, \phi)| \\ &= \sqrt{[x(t) - x(\tau)]^2 + [y(t)\cos(\theta) - y(\tau)\cos(\phi)]^2 + [y(t)\sin(\theta) - y(\tau)\sin(\phi)]^2} \\ &= (a(t, \tau) - b(t, \tau) \, \cos(\theta - \phi))^{\frac{1}{2}} \end{aligned} \tag{12}$$

with

$$a(t,\tau) = (x(t) - x(\tau))^2 + y^2(t) + y^2(\tau) \tag{13}$$

$$b(t,\tau) = 2\, y(t)\, y(\tau) \tag{14}$$

Note that neither g nor φ depends on θ; we also obtain the axisymmetric Green's function, denoted by Ψ which is regarded as a function either of $\mathbf{x}, \mathbf{y}$ or of t, τ, by integrating (6)

$$\mathbf{\Psi}(t,\tau) = \frac{1}{4\pi} \int_0^{2\pi} \frac{e^{i\,k\,|\mathbf{x}-\mathbf{y}|}}{|\mathbf{x}-\mathbf{y}|} d\theta \tag{15}$$

where Ψ is independent of θ, ϕ due to the fact that $R(t,\tau,\theta,\phi) = |\mathbf{x}(t,\theta) - \mathbf{y}(\tau,\phi)|$ depends on $\theta - \phi$. Consequently and obviously, the boundary integral equation (3) on ∂D reduces to one on Γ

$$\varphi - K'\varphi - i\eta T\varphi = -2g \tag{16}$$

with $g = g(t)$ independent of θ. The operators K' and T are still defined by (4), (5) with Φ replaced by Ψ

$$(K'\varphi)(\mathbf{x}) = 2 \int_{\partial D} \frac{\partial \Psi(\mathbf{x},\mathbf{y})}{\partial \nu(\mathbf{x})} \varphi(\mathbf{y})\, ds(\mathbf{y}) \quad \mathbf{x} \in \partial D \tag{17}$$

$$(T\varphi)(\mathbf{x}) = 2 \frac{\partial}{\partial \nu(\mathbf{x})} \int_{\partial D} \frac{\partial \Psi(\mathbf{x},\mathbf{y})}{\partial \nu(\mathbf{y})} \varphi(\mathbf{y}) ds(\mathbf{y}), \quad \mathbf{x} \in \partial D \tag{18}$$

Note that now $\mathbf{x}$ and $\mathbf{y}$ are restricted on the curve Γ – in other words, they are given by (10) and (11) with $\theta = 0$.

2.4 Singularity in K' and its Quadrature Issues

In this section we will illustrate the difficulties experienced with the kernel of K' whose proper quadrature treatment is required for the Nyström method to discretize the boundary integral equation (16). Let's assume for simplicity that

k is not a Dirichlet eigenvalue in the interior of Γ; consequently, our scattering problem can still be solved with $\eta = 0$ which we assume for the time being, so that we never consider in this paper the quadrature issues involved in tackling the operator T.

As is well known, the kernels Ψ, K' have logarithmic singularity which, in the case of K', can always be written as

$$K'(t,\tau) = \ln\left(4\sin^2\frac{t-\tau}{2}\right) g_1(t,\tau) + g_2(t,\tau) \tag{19}$$

where g_j, as well as φ, are equally smooth as the curve Γ [4].

One of the most advanced methods to design a spectrally convergent quadrature for (4) and other more general singular integrals [5,6] does not require the knowledge of g_j, but calls for a solution of a nonlinear system of equations with extremely high condition number when the number of quadrature nodes n is large; therefore, its calculation must be carried out with extended precision and could be extremely time consuming for n exceeding 100.

On the other hand, the most simple and popular method to design a spectrally convergent quadrature for (4) is what we term as the corrected trapezoidal rule [4,7] which requires the explicit decomposition (19). Unfortunately, there has been no success in stabily computing the values of g_j required in the corrected trapezoidal rule; see, for example, [3], page 335. To be more precise, we found in our own numerical tests that recursions (4.4), (4.5) in [3] which are said to be "stable for k not too large", become unstable for ka greater than about 5, namely when the size of the scatterer is about a wavelength.

3 The Interpolation Method

We describe and test a systematic method for the solution of the exterior Neumann problem which is spectrally convergent and trivial to implement because there is no need of quadrature at all. Let's assume that k is not a Neumann eigenvalue in the interior of Γ; see §3.3. We will consider only a smooth curve Γ. We further require the knowledge of not the boundary value g but its sources: The monopoles and dipoles which produce g. More precisely, we require the ability to evaluate the incident wave or its first derivatives on the boundary Γ or in the domain Ω.

Remark 1 *Denote by G the free space Green's function for the scattering problem – it is $(i/4)H_0$ or e^{ikr}/r for the two or three dimensional scattering problem, it is Ψ of (15) for the axisymmetric scattering problem.*

Our method will determine the double layer density φ on Γ such that the scattered field v is given by

$$v(\mathbf{x}) = \int_\Gamma \frac{\partial G(\mathbf{x},\mathbf{y})}{\partial \nu(\mathbf{y})} \varphi(\mathbf{y}) ds(\mathbf{y}) \tag{20}$$

This very simple, and we think powerful, approach, whose coding is almost trivial – an exterior Neumann problem in two or three dimensions could be coded in a matter of hours – is not without side effects. It involves a solution of a basically first kind integral equation, and consequently the convergence stops at about 8 digits, for a double precision calculation. The culprit is of course the condition number which not only restricts the precision – by itself we don't think it is a practical problem – but also excludes the use of an iterative solver to deal with large scale problems. In three dimensions, the largest problem which can be solved directly is about 10-by-10 square wavelengths;

any problem substantially greater than that is prohibitive in CPU time of a workstation or PC. In two dimensions, the high condition number is not a practical problem, for example, for a scattering calculation of an axisymmetric scatterer for the acoustic horn simulation. We are able to solve such a problem with the boundary Γ of 1000 wavelengths, whereas an acoustic horn usually has a Γ of less than 100 wavelengths.

3.1 Continuity and Interpolation

Let u_0, u be the incident and total waves, and let v of (20) be the scattered wave so that

$$u = u_0 + v \tag{21}$$

Our method, equally applicable to two and three dimensions, is based on the two well known observations, one analytical the other numerical

Observation 2 *The normal derivative of the double layer potential (20) is continuous across the boundary* Γ*. Therefore, under the condition that* k *is not an interior Neumann eigenvalue, the unique solution* v *of (20) to our scattering problem is identical to the negative of the incident wave* u_0 *inside* Ω*.*

See, for example, [4] for a proof.

Observation 3 *Let* $\Omega \subset \mathbb{R}^2$ *be a domain with a smooth boundary* Γ *on which is laid an equispaced grid*

$$\Gamma_h = \{\mathbf{y}_j,\ j = 1, 2, \ldots, n\} \tag{22}$$

of grid size h*. Furthermore, denote by* γ *a curve inside* Ω *and parallel to* Γ *on*

which is laid an equispaced grid

$$\gamma_\hbar = \{\mathbf{x}_i,\ i = 1, 2, \ldots, m\} \tag{23}$$

of grid size $\hbar \leq h$. *Finally, denote by* K_h *the m-by-n matrix*

$$(K_h)_{ij} = \frac{\partial G(\mathbf{x}_i, \mathbf{y}_j)}{\partial \nu(\mathbf{y})} \tag{24}$$

Then the condition number of K_h *is bounded by about* 10^8 *and the double layer potential* v *of (20) on* $\gamma_\hbar$ *is approximated to a precision about* 10^{-8} *by the formula*

$$\tilde{u}(\mathbf{x}_i) = \sum_{j=1}^{n} G(\mathbf{x}_i, \mathbf{y}_j)\varphi_j, \quad x_i \in \gamma_\hbar \tag{25}$$

provided that the parallel curves Γ, γ *are separated by* $3.5h$ *for a sufficiently small* $h > 0$.

It follows immediately from the two observations that the double layer density φ of (20) on Γ can be obtained as the unique solution of the least squares problem

$$K_h\, \varphi_h = -u_0|_{\gamma_\hbar} \tag{26}$$

Remark 4 *The least squares problem can obviously be regarded as an discretization of the first kind integral equation (see (20))*

$$\int_\Gamma \frac{\partial G(\mathbf{x}, \mathbf{y})}{\partial \nu(\mathbf{y})} \varphi(\mathbf{y}) ds(\mathbf{y}) = -u_0(\mathbf{x}), \quad \mathbf{x} \in \gamma \tag{27}$$

with the notable exception that γ *is not fixed; it is dependent on* h, *and its separation from* Γ *vanishes as* $h \to 0$.

Remark 5 *An alternative viewpoint to that of Remark 4 maybe more revealing of our method. The linear least squares problem (26) is typical for data fitting or interpolation. Indeed, we determine the linear combination coeffi-*

cients φ_j so that the incident wave $-u_0$ is matched or interpolated at the m points $\mathbf{x}_i$ on the curve γ in the least squares sense by using the basis functions

$$B_j(x) = \frac{\partial G(\mathbf{x}, \mathbf{y}_j)}{\partial \nu(\mathbf{y})} \tag{28}$$

Hence the term "solving the boundary integral equation by interpolation".

Remark 6 *According to Observation 3, the interpolation is accomplished with about 10^{-8} precision. This does not always guarantee that φ_j will be obtained with the same precision – a lower precision occurs when the local curvature of Γ becomes much greater than the average. Our numerical experiments show, however, that the scattered wave $v(\mathbf{x})$ in the exterior of Ω has about the same precision 10^{-8} provided that $\mathbf{x}$ is separated from Γ at least by the same distance by which Γ and γ are separated – about $3.5h$ (see §4.7 for a numerical example).*

3.2 Generalizations of the Interpolation Method

We make a few more remarks on the generalizations of the interpolation method.

Remark 7 *The grid size h does not have to be uniform. For a graded mesh, h measures the local density of the sampling grid points; therefore for a graded mesh, γ will not be parallel to the boundary Γ – they become closer where Γ is oversampled. Fortunately, our experiments show that Observation 3 is still basically true. In §4.7, we present numerical evidence to support this claim.*

Remark 8 *The entire discussion and approach presented in §3.1 is obviously generalizable to three dimensions where we assume that the surface Γ is sampled with a mesh which is locally as close to a square of size h-by-h as possible*

for some $h > 0$. It is then this h that defines the local separation of the two "parallel" surfaces Γ and γ. We found in our experiments that the choice of the sampling points for interpolation, just as any distribution of points for interpolation, is extremely flexible as long as the basic requirement for density of sampling is met. It is extremely resilient to the abuse of arbitrary oversampling. This flexibility marks a noticeable difference between the points for interpolation and those for the quadratures: The former is analytically based and is perturbable whereas the latter is algebraically based and is rigid – a small perturbation to the distribution of the quadrature nodes may utterly change the nature of the process, usually rendering it low order or useless.

Remark 9 *The assumption that k is not a Neumann eigenvalue in the interior of Ω does not exclude the possibility that k is a Dirichlet eigenvalue in the interior of γ. When this happens or nearly happens, an incident wave u_0 not identically zero may be zero or nearly zero on γ, which is analytically or numerically problematic since the least squares problem will produce a zero or nearly zero solution φ. As is well known [4], the impedance condition on γ*

$$u_0 + i\,\mu \frac{\partial u}{\partial \nu}, \quad \mu \in \mathbb{R}^1 \text{ is a parameter} \tag{29}$$

never vanishes or becomes small relative to $\|u_0\|_2$ on Ω, and will be used to perform the interpolation

$$(K_h + i\,\mu\, T_h)\,\varphi_h = -\left(u_0 + i\,\mu \frac{\partial u}{\partial \nu}\right)|_{\gamma_h} \tag{30}$$

with T_h the m-by-n matrix

$$(T_h)_{ij} = \frac{\partial^2 G(\mathbf{x}_i, \mathbf{y}_j)}{\partial \nu(\mathbf{x}) \partial \nu(\mathbf{y})} \tag{31}$$

3.3 Interpolation for Resonant k

If k is a Neumann eigenvalue in the interior of Ω, the representation (20), as is well known, becomes inadequate. This can be easily resolved using the so-called representation theory approach [4]. Taking the two dimensional case for example, we represent the scattered wave v in $\mathbb{R}^2 \setminus \Omega$ with its Dirichlet and Neumann data on Γ via Green's second theorem

$$v(\mathbf{x}) = \int_\Gamma \left[\frac{\partial G(\mathbf{x}, \xi)}{\partial \nu_\xi} v(\mathbf{y}) - G(\mathbf{x}, \mathbf{y}) g(\mathbf{y}) \right] ds(\mathbf{y}), \quad x \in \mathbb{R}^2 \setminus \Omega \tag{32}$$

Therefore, for prescribed Neumann data g, we only need to determine the Dirichlet data $v|_\Gamma$. Since the right hand side of (32) vanishes for $\mathbf{x} \in \Omega$, it also vanishes on γ, and we thus obtain

$$\int_\Gamma \frac{\partial G(\mathbf{x}, \xi)}{\partial \nu_\xi} v(\mathbf{y})\, ds(\mathbf{y}) = \int_\Gamma G(\mathbf{x}, \mathbf{y}) g(\mathbf{y})\, ds(\mathbf{y}), \quad x \in \gamma \tag{33}$$

Let $f : \gamma \mapsto \mathbf{C}$ be defined by

$$f(\mathbf{x}) = \int_\Gamma G(\mathbf{x}, \mathbf{y}) g(\mathbf{y})\, ds(\mathbf{y}) \tag{34}$$

Once f is sampled on $\gamma_\hbar$, which requires a quadrature but for smooth functions, it remains to apply the interpolation method in order to determine the Dirichlet data $v|_\Gamma$.

4 Numerical Results for Axisymmetric Case

We summarize in §4.1–4.4 a few points on implementing the interpolation method applied to the case of sound hard, smooth, axisymmetric scatterers illuminated by axisymmetric incident waves. We will demonstrate the performance of our method with three examples in §4.5–4.7. For simplicity, we will

only treat the nonresonant case: k is not a Neumann eigenvalue interior of Ω. The resonant case can be analogously handled; see §3.3.

4.1 Sample the boundary curve Γ

The smooth curve Γ, in the xy plane whose rotation around the x-axis form the axisymmetric scattering body, is usually discretized, or sampled with equispaced points in arclength. Due to the interpolation nature of the discretization, the points may be equispaced in chord-length to give essentially the same numerical performance. Moreover, they don't have to be exactly equispaced in arclength or chord-length, just as for interpolation on the interval $[-1, 1]$, the Chebyshev points are essentially as good as the Legendre points, or, say, Legendre points plus a point in some arbitrary location in $[-1, 1]$ – an abuse in the sampling will not have any noticeable effect on the least squares problem as long as the object is sampled with an adequate rate.

Local mesh refinement can also be arbitrarily added as necessary without further concern. If an incident source point outside Γ is close to it, we must locally sample Γ with a step size h that is no greater than $1/4$ of the separation.

4.2 Sample the parallel curve γ

The parallel curve γ (see Observation 3) need not be created; only the grid points $\gamma_\hbar$ are required for interpolation. For any point $\mathbf{y}_j$ on Γ_h and for small h compared to the radius of curvature at $\mathbf{y}_j$, consider the chord segment $\overline{\mathbf{y}_j\mathbf{y}_{j+1}}$. Move this segment in the inward normal direction by a distance $3.5h$, and on it we can choose a point $\mathbf{x}_i$ for the grid $\gamma_\hbar$. For a given h adequate to sample

Γ, our experiments show that $\hbar = h/1.4$ is about sufficient to sample γ.

4.3 The discretized linear system

It follows from (27) that our discretized linear system is

$$\sum_{j=1}^{n} \frac{\partial G(\mathbf{x}_i, \mathbf{y}_j)}{\partial \mathbf{n}(\mathbf{y}_j)} \varphi_j = u_0(\mathbf{x}_i) \quad i = 1, 2, \ldots, m; \quad \mathbf{x}_i \in \gamma_\hbar, \quad \mathbf{y}_j \in \Gamma_h \tag{35}$$

where according to Remark 1

$$\frac{\partial G(\mathbf{x}_i, \mathbf{y}_j)}{\partial \mathbf{n}(\mathbf{y}_j)} = \int_0^{2\pi} \nabla \frac{e^{ikR(\mathbf{x}_i, \mathbf{y}_j)}}{R(\mathbf{x}_i, \mathbf{y}_j)} \cdot \mathbf{n}(\mathbf{y}_j)\, d\theta \tag{36}$$

and

$$\nabla \frac{e^{ikR(\mathbf{x}_i, \mathbf{y}_j)}}{R(\mathbf{x}_i, \mathbf{y}_j)} \cdot \mathbf{n}(\mathbf{y}_j) = \left[\frac{i\,ke^{ikR}}{R^2} - \frac{e^{ikR}}{R^3}\right] \left([x(t_j) - \gamma_i^x]\, n_x(t_j) + [y(t_j)\, n_y(t_j)] - [\gamma_i^y\, n_y(t_j)\, \cos\theta] \right) \tag{37}$$

$\mathbf{n}(\mathbf{y}_j) = (n_x(t_j), n_y(t_j))$ is the outward unit normal of Γ and $\mathbf{x}_i = (\gamma_i^x, \gamma_i^y)$ (see §4.2). Since (36) is a regular integral, it can be easily evaluated numerically via Gaussian quadrature or trapazoidal rule quadrature.

4.4 The least-squares solution

The entire axisymmetric scattering algorithm was implemented in 81 lines of Matlab code. The least squares solution is obtained using either SVD or the more efficient Householder QR with column pivoting; their solutions are almost identical. When the oversampling is required on Γ, the spectrum cutoff is done to 10^{-8}, again, either on SVD or on the column pivoted QR.

We also coded the algorithm in ANSI C. The CPU timings and numerical

convergence results presented in §4.5 – §4.7 are all based on the C code implementation.

4.5 Numerical Results: Sound Hard Sphere

As a first test of our algorithm, we compute the scattering off a sound hard sphere and compare it to the analytical series solution in order to verify accuracy.

The analytic solution of an incident wave V^i created by a point source at $\mathbf{r}_0 = (r_0, 0, 0)$ such that $V^i = \frac{e^{ikR}}{kR}$ scattering off a sound hard sphere is given by [8]:

$$V^i + V^s = i \sum_{n=0}^{\infty} (2n+1) P_n(\cos\theta) h_n^{(1)}(kr_>)[j_n(kr_<) - \frac{j_n'(ka)}{h_n^{(1)'}(ka)} h_n^{(1)}(kr_<)] \quad (38)$$

Where j_n,$h_n^{(1)}$, and P_n are spherical Bessel, spherical Hankel, and Legendre functions as defined in [9]:

$$j_n(x) \doteq \sqrt{\frac{\pi}{2x}} J_{n+\frac{1}{2}}(x) \quad (39)$$

$$h_n^{(1)}(x) \doteq \sqrt{\frac{\pi}{2x}} H_{n+\frac{1}{2}}^{(1)}(x) \quad (40)$$

and $'$ denotes the derivative:

$$j_n'(x) = -1/4\,\sqrt{2} J_{n+\frac{1}{2}}(x) \pi \frac{1}{\sqrt{\frac{\pi}{x}}} x^{-2} + 1/2\,\sqrt{2}\sqrt{\frac{\pi}{x}} \left(-J_{n+\frac{3}{2}}(x) + \frac{(n+1/2)\, J_{n+\frac{1}{2}}(x)}{x} \right) \quad (41)$$

$$h_n^{(1)'}(x) = -1/4\,\sqrt{2} H_{n+\frac{1}{2}}^{(1)}(x) \pi \frac{1}{\sqrt{\frac{\pi}{x}}} x^{-2} + 1/2\,\sqrt{2}\sqrt{\frac{\pi}{x}} \left(-H_{n+\frac{3}{2}}^{(1)}(x) + \frac{(n+1/2)\, H_{n+\frac{1}{2}}^{(1)}(x)}{x} \right) \quad (42)$$

and a is the radius of the sphere (centered at the origin).

Table 2 shows the convergence results as the number of points per wavelength λ increases for a problem of size $ka = 50$. Note that spectral convergence is clearly exhibited. Also, as expected, the convergence stops at about 8 digits.

4.6 Numerical Results: Sound Hard Torus

As our next example, we compute the scattering of a point source from a sound hard torus. The torus is formed by rotating a circle of radius 1 around the x–axis. Figure 1 shows the geometry of the example (curves Γ and γ), the location of the point source and the measurement location.

Table 1 shows the convergence results when $k = 25$.

4.7 Numerical Results: Sound Hard "Squashed" Elliptical Torus

In this section we describe the results from a point source scattering off of an elliptical torus. This example more closely resembles a more complicated geometry situation that is likely to arise in study the sound propagating through waveguides or musical horns. Figure 2 shows the curves Γ and γ that are rotated around the x–axis to form the surface–of–rotation.

Figure 3 shows a visualization of the magnitude of the total pressure field (in Decibels $20 \log_{10}(|u|)$).

Table 3 shows the numerical convergence results of this elliptical torus waveguide when $k = 5$, and Table 4 shows the numerical convergence results when

$k = 25$. The elipse Γ used was

$$\mathbf{y}_j = (3 + 3\,\cos(\theta_j), 3 + \sin(\theta_j)) \quad \theta_j = \frac{2\,\pi\,j}{n} \quad j = 1, 2 \ldots n \tag{43}$$

Consequently, h and $\hbar$ are not constant. The locations of the m interpolation points $\mathbf{x}_i$ on $\gamma_\hbar$ where located as described in §4.2 and were placed $3.5h$ inward from Γ. However, as noted in remark 7, we still get spectral convergence similar to the equispaced h cases §4.5, §4.6. We tried cases from $3h$ spacing up to $6h$ spacing and the convergence results are similar, with each different spacing producing a slightly modified balance between conditioning and accuracy.

Table 1

$k = 25$, Point Source at $(0, 0, 0)$ Scattering of a Torus: Convergence Results. Measurement at $(6, 0, 0)$. Timings on a Sun UltraSPARC–IIi 333MHz.

n	$\frac{\text{pts}}{\lambda}$	real$(6, 0, 0)$	imag$(6, 0, 0)$	cond(K_h)	sec
50	2	$-3.76367558 \times 10^{-1}$	$-5.24075879 \times 10^{-1}$	3.4×10^4	16
75	3	$-4.64249894 \times 10^{-1}$	$-4.19129969 \times 10^{-1}$	1.8×10^5	44
100	4	$-4.64249856 \times 10^{-1}$	$-4.19129371 \times 10^{-1}$	2.4×10^5	73
125	5	$-4.64249853 \times 10^{-1}$	$-4.19129380 \times 10^{-1}$	2.8×10^5	118

Table 2

Sound Hard Sphere Scattering Convergence Results. $k = 50$, $a = 1$, Point Source at $(2, 0, 0)$, measurement at $(-5, 0, 0)$. Timings on a Sun UltraSPARC–IIi 333MHz.

n	$\frac{\text{pts}}{\lambda}$	real$(-5, 0, 0)$	imag$(-5, 0, 0)$	cond(K_h)	sec
50	2	$-9.84952112163 \times 10^{-4}$	$2.08844578780 \times 10^{-3}$	2.9×10^3	6
75	3	$-2.17795860698 \times 10^{-3}$	$-1.99585308419 \times 10^{-3}$	2.9×10^5	16
100	4	$-2.17795858130 \times 10^{-3}$	$-1.99585302271 \times 10^{-3}$	7.0×10^5	29
125	5	$-2.17795858336 \times 10^{-3}$	$-1.99585303039 \times 10^{-3}$	1.1×10^6	49
150	6	$-2.17795858361 \times 10^{-3}$	$-1.99585302726 \times 10^{-3}$	1.5×10^6	73
analytic		$-2.17795858673 \times 10^{-3}$	$-1.99585302502 \times 10^{-3}$		

Table 3

Axisymmetric Sound Hard Elliptical Torus Convergence Results. $k = 5$

n	m	real$(10, 0, 0)$	imag$(10, 0, 0)$	cond(K_h)
31	37	$-2.399280909245101 \times 10^{0}$	$-3.837220105033818 \times 10^{-1}$	1.06×10^{3}
62	74	$-5.342195808937857 \times 10^{-1}$	$-2.107520916009695 \times 10^{-1}$	1.70×10^{6}
83	99	$-5.342286682748080 \times 10^{-1}$	$-2.107502726151059 \times 10^{-1}$	4.17×10^{5}
125	150	$-5.342286817192076 \times 10^{-1}$	$-2.107502839740987 \times 10^{-1}$	9.29×10^{4}
251	301	$-5.342286806187949 \times 10^{-1}$	$-2.107502826867724 \times 10^{-1}$	4.69×10^{4}

Table 4

Axisymmetric Sound Hard Elliptical Torus Convergence Results. $k = 25$

n	m	real$(10, 0, 0)$	imag$(10, 0, 0)$	cond(K_h)
125	150	$-6.056849086854506 \times 10^{-1}$	$-2.285777494365712 \times 10^{0}$	5.09×10^{4}
251	301	$5.951955487916392 \times 10^{-1}$	$-1.678901006004439 \times 10^{0}$	3.27×10^{4}
502	602	$5.951955918630742 \times 10^{-1}$	$-1.678901075986008 \times 10^{0}$	3.73×10^{4}
1005	1206	$5.951955908636510 \times 10^{-1}$	$-1.678901077850511 \times 10^{0}$	4.84×10^{4}
2010	2120	$5.951955908637675 \times 10^{-1}$	$-1.678901077850542 \times 10^{0}$	5.17×10^{4}

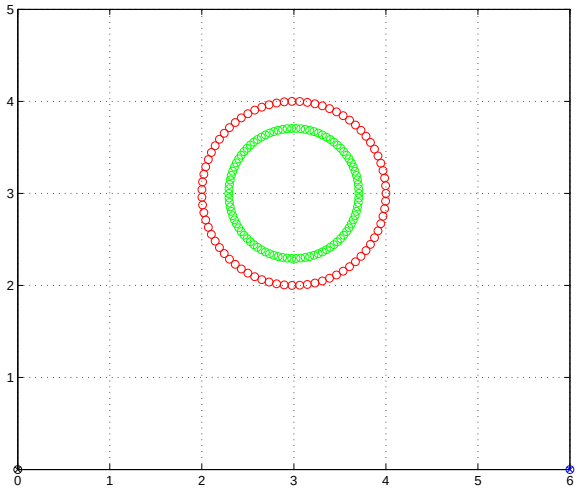

Fig. 1. The red points are the location of the n points $\mathbf{y}_j$ on Γ, and the green points are the m testing locations $\mathbf{x}_i$ on γ. The $\mathbf{x}_i$ points are located a distance $3.5h$ from $\mathbf{y}_j$. When rotated around the x–axis, the surface–of–rotation is a torus.

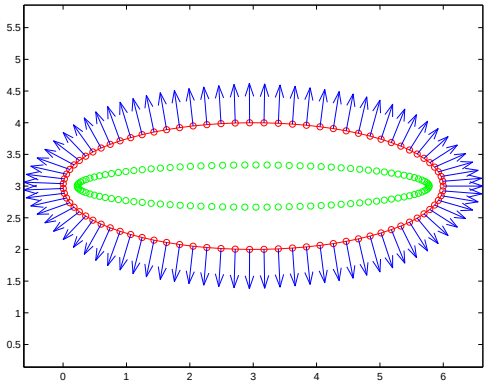

Fig. 2. This figure shows the geometry of the elliptical torus waveguide defined by rotating the the red ellipse around the x–axis. The red points are the location of the n points $\mathbf{y}_j$ on Γ, and the green points are the m testing locations $\mathbf{x}_i$ on γ. The $\mathbf{x}_i$ points are located a distance $3.5h$ from $\mathbf{y}_j$. The blue arrows show the outward unit normals $\mathbf{n}(\mathbf{y}_j)$.

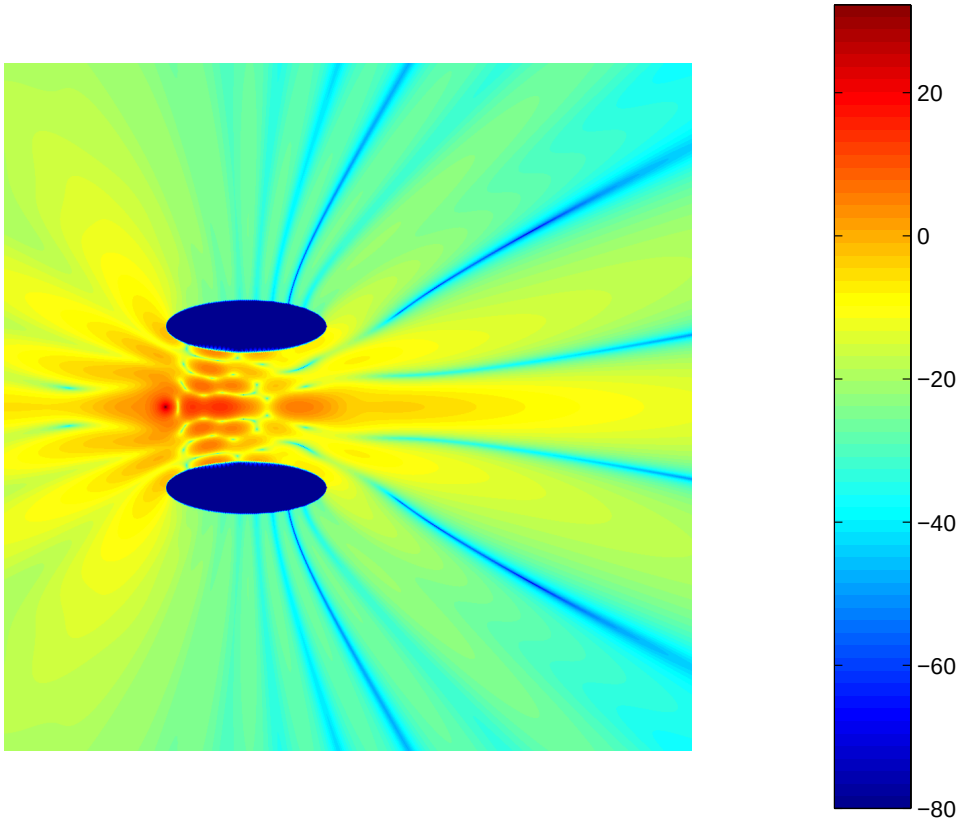

Fig. 3. A visualization of the total field from a point source scattering through the elliptical torus waveguide defined in figure 2. The dimensions are 12 by 12. k = 5. The colormap shows the magnitude of the total pressure field in Decibels.

References

[1] O. P. Bruno, L. A. Kunyansky, Fast, high-order solution of surface scattering problems, in: A. B. et al. (Ed.), Fith International Conference on Mathematical and Numerial Aspects of Wave Propagation, Society for Industrial and Applied Mathematics, 2000, pp. 465–470.

[2] L. F. Canino, J. J. Ottusch, M. A. Stalzer, J. L. Visher, S. M. Wandzura, Numerical solution of the Helmholtz equation in 2d and 3d using a high–order Nystrom discretization, Journal of Computational Physics 146 (1998) 627–663.

[3] R. Kress, On constant alpha force–free fields in a torus, Journal of Engineering Mathematics 20 (1986) 323–344.

[4] D. Colton, R. Kress, Inverse Acoustic and Electromagnetic Scattering Theory, Second Edition, Springer–Verlag, Berlin, 1998.

[5] H. Cheng, V. Rokhlin, N. Yarvin, Nonlinear optimization, quadrature, and interpolation, SIAM J OPTIMIZ 9 (4) (1999) 901–923.

[6] N. Yarvin, V. Rokhlin, Generalized gaussian quadratures and singular value decompositions of integral operators, SIAM J SCI COMPUT 20 (2) (1998) 699–718.

[7] S. Kapur, V. Rokhlin, High-order corrected trapezoidal quadrature rules for singular functions, SIAM Journal of Numerical Analysis 34 (4) (1997) 1331–1356.

[8] J. J. Bowman, T. Senior, P. Uslenghi (Eds.), Electromagnetic and Acoustic Scattering by Simple Shapes, North Holland, Amsterdam, 1969.

[9] M. Abramowitz, I. A. Stegun (Eds.), Handbook of Mathematical Functions With Formulas, Graphs, and Mathematical Tables, Dover, New York, N.Y., 1972.